Engineering Fracture Mechanics 204 (2018) 268–287

Contents lists available at ScienceDirect

Engineering Fracture Mechanics

journal homepage: www.elsevier.com/locate/engfracmech

An iteration scheme for phase field model for cohesive fracture and its implementation in Abaqus

Peng Zhang[a,c], Xiaofei Hu[a,c,*], Xiaoyi Wang[b], Weian Yao[a,c]

[a] State Key Laboratory of Structural Analysis for Industrial Equipment, Dalian University of Technology, Dalian 116024, PR China
[b] Beijing Institute of Structure and Environment Engineering, Beijing, PR China
[c] International Research Center for Computational Mechanics, PR China

ARTICLE INFO

Keywords:
Phase field model
Cohesive fracture
Iteration scheme
Abaqus
UEL

ABSTRACT

Recently, phase field modelling of fracture has gained much attentions because of its benefits in predicting cracks initiation and propagation without any *ad-hoc* criterion. In the model cracks are smeared into the surrounding areas by introducing an auxiliary crack phase field which should be solved either by iteration or using sufficiently small loading increment, and this makes the method be computationally demanding. The introduction of other complex models e.g. cohesive zone model results in nonlinear damage sub-problems which may further increase the number of iteration steps. In this study, an improved staggered iteration scheme by which the nonlinear sub-problems are solved by a one-pass procedure is proposed. Such that the computational costs can be reduced and the stability of iteration can be improved. In particular, a unified phase field model which integrates varies cohesive relationships is investigated. The phase field model as well as the iteration scheme are implemented through Abaqus subroutine UEL (user defined element). The present study is validated through comparing both of crack propagation path and load-displacement curve with existing results. Moreover, comparisons on total iteration steps and the elapsed total computational time are made between the proposed iteration scheme and the existing scheme, and the results demonstrate that the proposed iteration scheme is very suitable for the considered problem.

1. Introduction

Simulation of crack initiation and propagation is very important for engineering structures. One of the main difficulties in the numerical simulations is to track the crack's geometry during propagation. The existing methods for modeling fracture problems can be generally divided into two categories: discrete crack models and smeared crack models. In discrete crack models, the crack is explicitly modeled either by pre-definition such as cohesive element method [1,2] or by tracking the crack location during the simulation such as extended finite element method [3,4]. However, difficulties such as proper methods to model curved crack fronts in three-dimensional (3D) fracture problems still exist. Hence smeared crack methods are put forward. In the model the discontinuity is represented by a smooth continuous field. The smeared discontinuity is accompanied with a specified stress-strain relationship in which the limit strength is gradually reduced. As pointed out in Ref. [5], this locally strain softening may result in a loss of well-posedness of the rate boundary value problem and the results may be sensitive to both mesh refinement and mesh alignment. To

* Corresponding author at: State Key Laboratory of Structural Analysis for Industrial Equipment, Dalian University of Technology, Dalian 116024, PR China.
E-mail address: hxf@dlut.edu.cn (X. Hu).

https://doi.org/10.1016/j.engfracmech.2018.10.006
Received 8 May 2018; Received in revised form 4 October 2018; Accepted 7 October 2018
Available online 13 October 2018
0013-7944/

overcome these difficulties a class of gradient-enhanced damage models were developed and becoming popular in computational analysis [6–9]. Recently, Nguyen et al. [10] proposed a novel smooth gradient damage model which is particularly tailored to low-order finite elements and can accurately predict the localized failure in quasi-brittle materials. In the smoothing gradient damage model a modified evolving anisotropic nonlocal gradient parameter was introduced to eliminate spurious damage growth and correct wrong prediction of shear band. Moreover, to precisely capture the softening in quasi-brittle materials, Nguyen et al. [10] also proposed a novel bi-energy norm. Another class of widely used smeared crack model termed as phase field model was developed from the variational formulation of brittle fracture proposed by Francfort and Marigo [11]. The model can overcome some limitations in the classical Griffith's theory [12] such as unable to predict the crack's nucleation, branching and curved propagation path. Bourdin et al. [13] used a scalar parameter (i.e. phase field) to regularize the sharp crack geometry into a diffusive entity. Kuhn and Müller [14] introduced a phase field evolution equation and stated that phase field model can be applied for brittle fracture simulation while the irreversible character of crack propagation is taken into account. Then this model was widely used for brittle fracture problems [15–19]. By decomposing the stored energy into the elastic and plastic parts, phase field model can be extended into ductile fracture problems [20–25]. Phase field model was also extended for dynamic fracture problems [26–34] based on the assumption that phase field has no influence on the kinetic energy and the fracture energy is independent of the crack velocity. Unlike these models, Doan et al. proposed a rate-dependent hybrid phase field model for dynamic fracture problems and confirmed that the rate-dependent coefficient plays an important role and must be taken into account in the analysis [35]. Phase field model and its application has been reviewed in Ref. [36].

Cohesive model based crack has been widely used in engineering, and its realization through phase field model is also interesting. In Refs. [37,38], a phase field model was proposed in which an auxiliary field to incorporate cohesive tractions. A variational formulation for cohesive fracture was proposed and investigated numerically in Refs. [39,40]. Recently, Wu proposed a non-standard unified phase field model for quasi-brittle failure [41–43]. Comparing with standard phase field models of brittle fracture [13,44,45], this unified model uses parameterized degradation and crack geometric functions. With a set of optimal characteristic functions, the widely used cohesive laws such as linear, exponential, hyperbolic and Cornelissen's softening models can be reproduced or approximated with high precision. For these crack models, nonlinear sub-problems are introduced due to the fact that crack traction and separation are not known *a priori*. All the parameters that are involved in the model can be determined through material properties such as Young's modulus, fracture strength, fracture energy and the adopted cohesive law. Another significant improvement of the model is that the structure response is insensitive to the internal length scale [41–43,46]. By now the unified phase field model has already been successfully extended to model brittle fracture problems [47] and dynamic fracture problems [48].

In phase field model for fracture problem the displacement field and crack phase field in the governing equations are both unknown. The discretized governing equations are usually solved by means of incremental method. During each load increment, either monolithic scheme [32,45] or staggered scheme [15,16,19] is employed to calculate the unknown variables. In the former scheme [32,45], the Newton-Raphson iteration form is constructed directly from the weak form of the governing equation. This scheme is efficient as it solves displacement and crack phase field simultaneously in one loop of iterations [16]. In order to reduce programming work and make the advanced diffusive crack model widely available for scientists and engineers, Msekh et al. implemented the model with monolithic scheme into commercial software Abaqus through user's subroutine UEL [17]. However, due to the fact that the system's energy functional is not convex, this monolithic scheme usually demands very small load increments to get a convergent solution and sometimes convergence issue still exists for complex fracture problems. In staggered scheme, the system is split into two independent minimization problems, i.e. the displacement problem and phase field problem. Then the discretized governing equations are solved by fixing displacement of phase field alternatively. This scheme was proven to be robust [15]. In Ref. [16] Ambati et al. proposed a hybrid formulation of the phase field model. With this formulation the nested iteration, which is caused by the separation of strain energy, in the staggered scheme can be avoid. Numerical results indicated that the computational cost was reduced about one order of magnitude [16]. In Ref. [19] Molnár et al. proposed a slightly different staggered scheme for phase field modeling of brittle fracture problems. It is found that this kind of staggered scheme actually has the same convergent path with the scheme in Refs. [15,16] and very suitable for Abaqus implementation. However, these solution algorithms are originally proposed for standard phase field model of brittle fracture [13,44,45]. And for phase field model for cohesive cracking [41,42] since the cohesive traction and separation are not known *a priori*, the phase field sub-problem is no longer linear when the staggered iteration scheme is used. Additional computational costs are hence needed and sometime convergence issue may occur for complex problems as shown in the numerical example of Section 6.4.

In this paper, an improved staggered iteration scheme for phase field models with nonlinear phase field sub-problem is proposed. A one-pass scheme for nonlinear sub-problem is introduced to avoid additional iteration efforts and hence the computational expense is reduced. It is noteworthy that the proposed iteration method degenerates to standard staggered iteration scheme for phase field models without any nonlinear sub-problem. The iteration path is shown in Section 4. In particular, the unified model for cohesive cracks [41,42] is employed for the investigation of quasi-brittle fracture. The numerical examples of these papers are reconsidered with different iteration schemes to validate the proposed method. The hybrid formulation [16] is adopted here to avoid the nested iterations caused by the decomposition of the strain tensor. Theoretically, the phase field model as well as the iteration scheme can be implemented into any finite element package. In this study, the proposed method is implemented into Abaqus through the user subroutine user defined element (UEL). By using the preprocessor and nonlinear analysis solver of Abaqus, the multi-field problem can be solved more efficiently. The programming work is reduced, only the finite element formulation has to be implemented. It will surly increase the programming efficiency comparing with in-house FEM codes. Moreover, the source codes of the UEL is provided in Appendix as supplementary material in order to make the model widely available for not only scientific research but also practical applications. As long as the computer has installed the commercial software Abaqus and Fortran compiler, the provided UEL codes

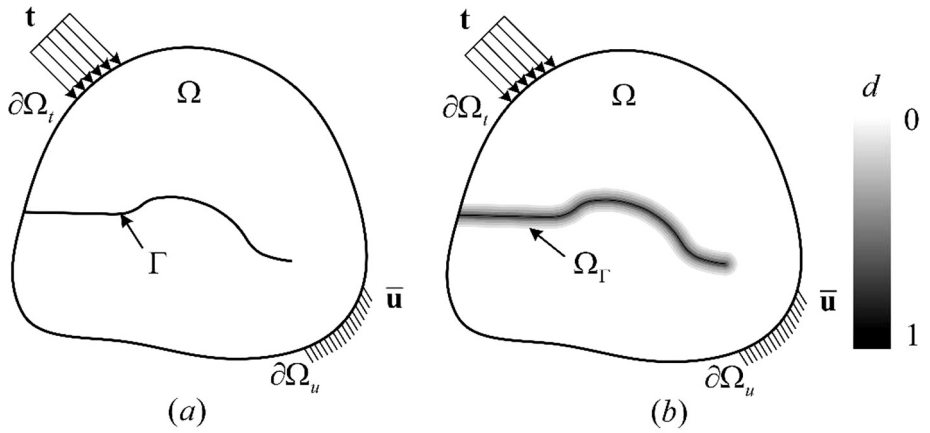

Fig. 1. (a) A body with crack inside. (b) Illustration of smeared cracks.

can be run with slight modifications.

2. Phase field model

2.1. Governing equations

As shown in Fig. 1, the discrete crack is represented by a discontinuity boundary Γ. According to the Francfort-Marigo framework [11], the total energy of the domain Ω is given by

$$\psi = \int_\Omega \mathbf{f}\cdot\mathbf{u}\mathrm{d}V + \int_{\partial\Omega_t} \mathbf{t}\cdot\mathbf{u}\mathrm{d}S - \int_{\Omega\setminus\Gamma} \psi^e \mathrm{d}V - \int_\Gamma G_s \mathrm{d}S \tag{1}$$

where $\mathbf{u}$ is the displacement field in Ω, ψ^e is the strain energy density in intact area, and G_s is the critical energy release rate, $\mathbf{f}$ is the body force and $\mathbf{t}$ is the applied traction in boundary $\partial\Omega_t$.

The variational approach of fracture proposed by Francfort and Marigo convert the crack's nucleation and propagation problem into a global energy minimizer problem. But since the discontinuity boundary Γ is changing with time, significant difficulty is met in solving the variational problem numerically. To overcome this difficulty, as shown in Fig. 1, Bourdin et al. [13] regularized the discrete crack by a continuity scale field d (i.e. phase field). The phase field is varying from 0 at the intact material state to 1 at the totally damaged state. Then a crack surface density function γ determined by phase field can be introduced naturally [41].

$$\gamma(d,\ \nabla d) = \frac{1}{c_0}\left(\frac{1}{l_0}\alpha(d) + l_0\ |\nabla d|^2\right) \tag{2}$$

where l_0 is the internal length scale regularizing the sharp crack, $\alpha(d)$ is the geometric function characterized homogeneous evolution of the phase field [45] and $c_0 = 4\int_0^1 \sqrt{\alpha(d)}\,\mathrm{d}d$. So the potential energy can be rewritten as

$$\psi = \int_\Omega \mathbf{f}\cdot\mathbf{u}\mathrm{d}V + \int_{\partial\Omega_t} \mathbf{t}\cdot\mathbf{u}\mathrm{d}S - \int_\Omega \omega(d)\psi^e \mathrm{d}V - \int_{\Omega_\Gamma} \gamma(d,\ \nabla d) G_s \mathrm{d}V \tag{3}$$

where $\omega(d)$ is an energy degradation function to describe the energy density degradation when the point is damaged ($d > 0$). And it should satisfy the following requirements [45]

$$\omega(0) = 1, \quad \omega(1) = 0 \tag{4}$$

$$\omega'(d) < 0, \quad \omega'(1) = 0 \tag{5}$$

By taking the variation of the potential energy function ψ, the corresponding strong form for the displacement and phase field can be written as

$$\begin{cases} \omega(d)\nabla\sigma + \mathbf{f} = 0 & in\ \ \Omega \\ \omega(d)\sigma\cdot\mathbf{n} = \mathbf{t} & in\ \ \partial\Omega_t \end{cases} \tag{6}$$

$$\omega'(d)\mathcal{H} + G_s\frac{1}{c_0}\left[\frac{1}{l_0}\alpha'(d) - 2l_0\Delta d\right] = 0 \quad in\ \ \Omega_\Gamma \tag{7}$$

where

$$\mathcal{H} = \max_{\tau\in[0,t]} \psi^+(\varepsilon(\mathbf{x},\tau)) \tag{8}$$

is a history-depended variable to enforce the phase field's irreversibility [45]. $\psi^+(\varepsilon)$ is the tension part of the initial strain energy density $\psi^e(\varepsilon)$ which is used to prevent cracking under compression state. And there are some alternatives for the definition of $\psi^+(\varepsilon)$ such as the energy split models in Refs. [45,49–51]. In the present study, the split operation (Miehe et. al., [45]) is used

$$\psi^{\pm} = \frac{\lambda}{2}\langle \boldsymbol{tr}(\varepsilon)\rangle_{\pm}^2 + \mu \boldsymbol{tr}(\varepsilon_{\pm}^2) \tag{9}$$

where λ and μ are lame constants, and $\langle\bullet\rangle$ is defined as $\langle x\rangle_{\pm} = (x \pm |x|)/2$.

2.2. Phase field model for cohesive fracture

In the governing Eqs. (6) and (7) there are two undetermined functions i.e. energy degradation function $\omega(d)$ and the geometric crack function $\alpha(d)$. In standard phase field model of brittle fracture [13,44,45] quadratic forms of degradation and geometric crack functions in the forms of

$$\omega(d) = (1-d)^2 \quad \textbf{\textit{and}} \quad \alpha(d) = d^2 \tag{10}$$

are usually adopted. However, as can be seen from the phase field evolution equation that a quadratic geometric crack function will lead to damage occurs under very low stress level. So in Refs. [9,52,53] a linear geometric crack function $\alpha(d) = d$ was used which can restore the elastic state of the material before damage nucleation. However, all the remedies were made for brittle fracture problems and for cohesive zone based crack models the situation become challenging. So in Ref. [41] Wu proposed a unified phase field model which can restore the cohesive laws. Unlike the tradition phase field model, in this unified model the following parametric degradation function $\omega(d)$ and geometric crack function $\alpha(d)$ are adopted [41]

$$\omega(d) = \frac{(1-d)^p}{(1-d)^p + Q(d)}, \qquad Q(d) = a_1 d + a_1 a_2 d^2 + a_1 a_2 a_3 d^3 + \cdots \tag{11}$$

$$\alpha(d) = \xi d + (1-\xi) d^2 \tag{12}$$

where ξ is an non-negative parameter ranging from 0 to 2, $p > 0$ and the coefficients a_i are calculated from material properties. In Ref. [41] the geometric function with $\xi = 2$ is adopted, then Eq. (12) can be rewritten as

$$\alpha(d) = 2d - d^2 \tag{13}$$

With the stress degradation function (11) and geometric function (13), in 1-D case the stress σ and the apparent displacement jump w across the localization failure band can be given as [41]

$$\sigma(d^*) = f_t \sqrt{\frac{(2-d^*)(1-d^*)^p}{2P(d^*)}} \tag{14}$$

$$w(d^*) = \frac{4\sqrt{2}G_s}{\pi f_t} \int_0^{d^*} \left[\frac{P(d^*)}{(1-d^*)^p} \frac{2-d}{2-d^*} - \frac{P(d)}{(1-d)^p} \right]^{-\frac{1}{2}} \frac{\sqrt{d}\,P(d)}{(1-d)^p} \mathrm{d}d \tag{15}$$

where d^* is the maximum phase field value obtained at the symmetric point $x = 0$, f_t is the cohesive strength, p is the order in Eq. (11) and $P(d) = 1 + a_2 d + a_2 a_3 d^2 + \cdots$. It can be seen that the stress and apparent displacement jump in Eqs. (14) and (15) has defined a general softening law. After some mathematic derivations the initial slop k_0 of the softening curve $\sigma(w)$ and the critical crack opening displacement w_c can be given as [41]

$$k_0 = -\frac{1}{16}\frac{f_t^2}{G_s}[2(a_2 + p) + 1]^{3/2} \tag{16}$$

$$w_c = \frac{2G_s}{f_t}\sqrt{2P(1)} \lim_{d^* \to 1} (1-d^*)^{1-p/2} \tag{17}$$

For a cubic form of $Q(d)$ in Eq. (11), the corresponding parameters can be determined and specified by [41]

$$a_1 = \frac{4}{\pi l_0}\frac{EG_s}{f_t^2} \tag{18}$$

$$a_2 = 2\left(-2k_0\frac{G_s}{f_t^2}\right)^{\frac{2}{3}} - \left(p + \frac{1}{2}\right) \tag{19}$$

$$a_3 = \begin{cases} 0 & when\ p > 2 \\ \frac{1}{a_2}\left[\frac{1}{8}\left(\frac{w_c f_t}{G_s}\right)^2 - (1+a_2)\right] & when\ p = 2 \end{cases} \tag{20}$$

It is seen that a_1 is determined once all the material parameters are specified, and the other parameters p, a_2 and a_3 used in Eq. (11) can be modified to represent specific cohesive zone models. For some typical cohesive zone models, the corresponding values of these

parameters are available and specified as follows [41]:

Linear softening relationship:

$$p = 2, \quad a_2 = -\frac{1}{2}, \quad a_3 = 0 \tag{21}$$

Exponential softening relationship:

$$p = \frac{5}{2}, \quad a_2 = 2^{5/3} - 3, \quad a_3 = 0 \tag{22}$$

Hyperbolic softening relationship:

$$p = 4, \quad a_2 = 2^{7/3} - 4.5, \quad a_3 = 0 \tag{23}$$

Cornelissen et al. [54] softening relationship:

$$p = 2, \quad a_2 = 1.3868, \quad a_3 = 0.6567 \tag{24}$$

In this study, only the Cornelissen softening cohesive zone model is considered

Substituting Eqs. (11) and (12) into Eq. (7), a new phase field evolution equation which can take into account the specified cohesive law is obtained. Unlike traditional phase field model with Eq. (10), the obtained evolution equation is no longer linear which will introduce additional iteration efforts and increase the computational expense for standard staggered iteration scheme. The damage boundedness $d \in [0, \ 1]$ is intrinsically guaranteed in the traditional phase field model with $\alpha(d) = d^2$. However, by adopting the new form of geometric crack function (12) the damage boundedness is no longer guaranteed. From the phase field evolution equation it can be seen that if the history variable defined in Eq. (8) is used, the lower limit of damage will be smaller than 0 which is physically unreasonable. In order to solve this issue, a modified history variable $\mathcal{H}$ is introduced as specified by

$$\mathcal{H} = \max_{\tau \in [0,t]} [\psi^+(\varepsilon(\mathbf{x}, \tau)), \quad \psi^0] \tag{25}$$

where

$$\psi^0 = -G_s \frac{\alpha'(0)}{\omega'(0) c_0 l_0} \tag{26}$$

is the critical energy that corresponds to a zero phase field. The phase field starts to evolve only if the strain energy density has reached this critical value. If $\alpha(d) = d^2$ is adopted for Eq. (26), then ψ^0 is equal to zero which means that in such circumstance Eq. (25) and equation are (8) equivalent with each other. Hence the new history variable (25) is unified for both standard and non-standard phase field models.

3. Finite element formulation

Once the parameters are determined, the governing Eqs (6) and (7) can be solved numerically by FEM. In the framework of FEM the displacement field $\mathbf{u}$ and phase field d can be discretized by shape functions $\mathbf{N}^u$ and $\mathbf{N}^d$ respectively.

$$\mathbf{u} = \mathbf{N}^u \mathbf{u}^e, \quad d = \mathbf{N}^d \mathbf{d}^e \tag{27}$$

where $\mathbf{u}^e$ and $\mathbf{d}^e$ are the displacement and phase field values at element nodes. So the corresponding derivatives can be specified as follows

$$\varepsilon = \mathbf{B}^u \mathbf{u}^e, \quad \nabla d = \mathbf{B}^d \mathbf{d}^e \tag{28}$$

where the matrix $\mathbf{B}^u$ and $\mathbf{B}^d$ are formed from the derivatives of the shape functions. With Eq. (27) and (28) the corresponding residual forms of displacement field and phase field can be expressed by

$$\mathbf{R}^u = \int_{\Omega^e} \{\mathbf{N}^u\}^{\mathrm{T}} \cdot \mathbf{f} \mathrm{d}V + \int_{\partial\Omega_t^e} \{\mathbf{N}^u\}^{\mathrm{T}} \cdot \mathbf{t} \mathrm{d}S - \int_{\Omega^e} \omega(d) [\mathbf{B}^u]^{\mathrm{T}} \sigma \mathrm{d}V = \mathbf{0} \tag{29}$$

$$\mathbf{R}^d = \int_{\Omega_\Gamma^e} \left\{ -\omega'(d) \mathcal{H} \{\mathbf{N}^d\}^T - G_s \frac{1}{c_0} \left[\frac{1}{l_0} \alpha'(d) \{\mathbf{N}^d\}^{\mathrm{T}} + 2 l_0 [\mathbf{B}^d]^{\mathrm{T}} \nabla d \right] \right\} \mathrm{d}V = \mathbf{0} \tag{30}$$

4. Iteration algorithm

In staggered iteration scheme, the coupled system of Eqs. (29) and (30) are solved alternatively [15]. Displacement is solved through Eq. (29) by fixing phase field. Similarly, Eq. (30) is solved for phase field by fixing displacement. Repeat the staggered iteration attempts until converge. In order to make the iteration procedure more intuitive, two scalars $\widehat{u}$ and $\widehat{d}$, which are termed as the "scalar displacement" and "scalar crack phase field", are introduced to represent the vectors. Assume that $\widehat{u}$ and $\widehat{d}$ satisfy the equations in the form of Eqs. (29) and (30), the following relations can be obtained

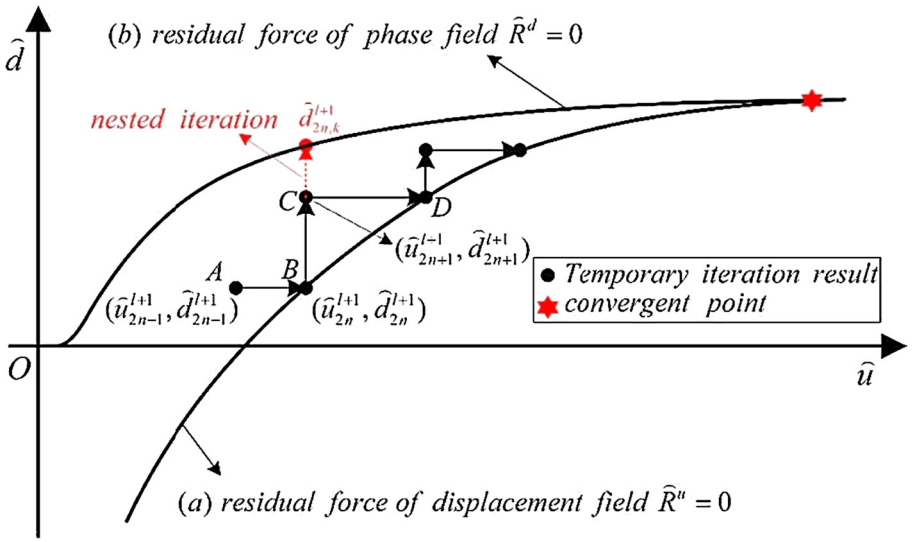

Fig. 2. Iteration procedure of the proposed iteration algorithm.

$$\widehat{R}^u = \widehat{P} - \omega(\widehat{d})\mathcal{A}\widehat{u} = 0 \tag{31}$$

$$\widehat{R}^d = -\omega'(\widehat{d})\mathcal{B}\widehat{u}^2 - \mathcal{E}\widehat{d} - \mathcal{F}\widehat{d} - C = 0 \tag{32}$$

In order to solve this nonlinear system of equation, the external loading is divided into several time increments. Without loss of generality, the $(l+1)$th time increment is considered to illustrate the iteration scheme.

In the $(l+1)$th load increment, two curves of $\widehat{u}$ and $\widehat{d}$ i.e., curves (a) and (b), which are obtained from Eqs. (31) and (32) are depicted in Fig. 2. Obviously, the cross point of these two curves is the convergence point of the present load increment. In this time step, iteration attempts are made for solving either displacement or phase field. Since these two variables are solved in a staggered manner, it is supposed that displacement is solved in odd iteration steps, i.e. $(2n-1)th$ step where $n = 1, 2, 3. \ldots$ So phase field is solved in even iteration steps i.e. $2nth$ step. Suppose the initial point locates at point A in Fig. 2, then according to the Newton-Raphson iteration scheme the scalar displacement $\widehat{u}$ in this iteration step is calculated through

$$\widehat{u}^{l+1}_{2n} = \widehat{u}^{l+1}_{2n-1} + \Delta\widehat{u}^{l+1}_{2n-1} \tag{33}$$

where

$$\Delta\widehat{u}^{l+1}_{2n-1} = (\widehat{K}^u_{2n-1})^{-1}\widehat{R}^u_{2n-1}, \qquad \widehat{K}^u_{2n-1} = -\frac{\partial\widehat{R}^u}{\partial\widehat{u}} = \omega(\widehat{d}^{l+1}_{2n-1})\mathcal{A} \tag{34}$$

and $\mathcal{A}$ is a constant calculated from Eq. (29). Since the value of $\mathcal{A}$ does not affect the illustration of the iteration procedure, the explicit form is not provided for the sake of simplicity. After this iteration step, the temporary result is moved from point A to point B in Fig. 2. Since the value of the scalar phase field $\widehat{d}$ is fixed, it is found that $\widehat{d}^{l+1}_{2n} = \widehat{d}^{l+1}_{2n-1}$. Then, in the next iteration step, phase field should be calculated through Eq. (30). However, this equation is nonlinear and a nested iteration procedure is required for standard staggered scheme. The incremental solution of the scalar phase field can be expressed as follows

$$\widehat{d}^{l+1}_{2n,k+1} = \widehat{d}^{l+1}_{2n,k} + \Delta\widehat{d}^{l+1}_{2n,k} \tag{35}$$

where

$$\Delta\widehat{d}^{l+1}_{2n,k} = (K^d_{2n,k})^{-1}R^d_{2n,k}, \qquad \widehat{K}^{l+1}_{2n,k} = -\frac{\partial\widehat{R}^d}{\partial\widehat{d}} = -\omega'(d^{l+1}_{2n,k})\mathcal{B}(\widehat{u}^{l+1}_{2n})^2 - \mathcal{E} - \mathcal{F} \tag{36}$$

The subscript k represents index of the nested iteration procedure. $\mathcal{B}$, $\mathcal{E}$ and $\mathcal{F}$ are constants which can be determined from Eq. (30). For the same reason as $\mathcal{A}$, the explicit forms of them are not provided for the sake of simplicity. In this step, the temporary result is moved from point B to point C. According to the above statements, a nested iteration procedure which is marked as the red dashed arrow above point C in Fig. 2 is required. But, it is found convergent result to the original problem can still be obtained even if the nested iteration procedure is omitted. This one-pass scheme will lead the temporary result from point C to D instead of moving along the red dashed arrow. Then repeat the iteration attempts until reaching the convergence point. Since the temporary results should always be constrained by the curve (a), a convergent result can be anticipated. And the one-pass scheme actually plays an important role in reducing computational expenses.

For phase field models for brittle fracture, the proposed iteration scheme degenerates into the widely used staggered scheme

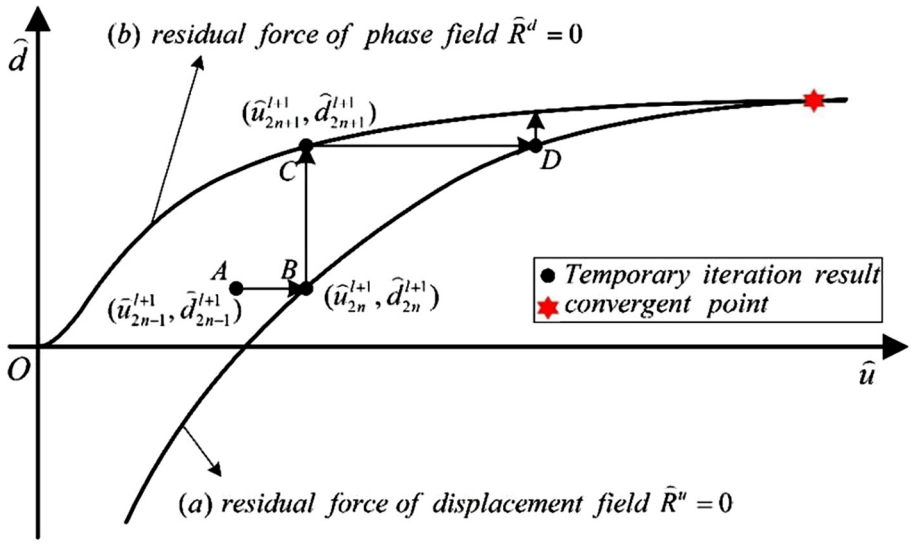

Fig. 3. Iteration procedure for brittle fracture problems.

[15,16]. In phase field models for brittle problems the geometric function $\alpha(d)$ and degradation function $\omega(d)$ are usually defined as

$$\alpha(d) = d^2, \quad \omega(d) = (1-d)^2 \tag{37}$$

Substituting these functions into Eq. (36) it can be seen that the tangential stiffness $\widehat{K}^{l+1}_{2n,k}$ is linear with respect to phase field. Which means that now the phase field problem also can be solved directly. The iteration steps are illustrated in Fig. 3. This iteration procedure is identical with the staggered scheme for brittle fracture problems used in Ref. [16].

Move back to the nonlinear system of Eqs. (29) and (30). Denote $\mathbf{u}^{l+1}_{2n-1}$, $\mathbf{d}^{l+1}_{2n-1}$ the values of the $(2n-1)$th iteration step in the $(l+1)$th load increment. Fixing phase field $\mathbf{d}^{l+1}_{2n-1}$, the problem can be solved through the following Newton-Raphson iteration form which is derived from Eq. (29)

$$\mathbf{u}^{l+1}_{2n} = \mathbf{u}^{l+1}_{2n-1} + \Delta\mathbf{u}^{l+1}_{2n-1} \tag{38}$$

where

$$\begin{aligned} \Delta\mathbf{u}^{l+1}_{2n-1} &= (\mathbf{K}^u_{2n-1})^{-1}\mathbf{R}^u_{2n-1} \\ \mathbf{K}^u_{2n-1} &= -\frac{\partial \mathbf{R}^u}{\partial \mathbf{u}^e} = \int_{\Omega^e} \omega(\mathbf{d}^{l+1}_{2n-1})[\mathbf{B}^u]^{\mathrm{T}}\mathbf{D}\mathbf{B}^u \mathrm{d}V \end{aligned} \tag{39}$$

Then, the obtained displacement field u^{l+1}_{2n} is fixed in the $2n$th iteration step and the phase field can be updated through

$$\mathbf{d}^{l+1}_{2n,k+1} = \mathbf{d}^{l+1}_{2n,k} + \Delta\mathbf{d}^{l+1}_{2n,k} \tag{40}$$

where

$$\begin{aligned} \Delta d^{l+1}_{2n,k} &= (\mathbf{K}^d_{2n,k})^{-1}\mathbf{R}^d_{2n,k} \\ \mathbf{K}^{l+1}_{2n,k} &= -\frac{\partial \mathbf{R}^d}{\partial \mathbf{d}^e} = \int_{\Omega^e_{\Gamma}} \omega''(\mathbf{d}^{l+1}_{2n,k})\mathcal{H}\mathbf{N}^d\{\mathbf{N}^d\}^{\mathrm{T}} + \\ & \quad G_s\frac{1}{c_0}\left[\frac{1}{l_0}\alpha''(\mathbf{d}^{l+1}_{2n,k})\mathbf{N}^d\{\mathbf{N}^d\}^{\mathrm{T}} + 2l_0[\mathbf{B}^d]^{\mathrm{T}}\mathbf{B}^d\right]\mathrm{d}V \end{aligned} \tag{41}$$

and $k = 0, 1, 2...$ is used to represent a nested iteration procedure. In order to avoid this problem, we apply the one-pass scheme here. That is to say in the present problem Eq. (40) is solved only once and the corresponding solution $\mathbf{d}^{l+1}_{2n,1}$ is used in the $(2n+1)$th iteration step. After a few steps a convergence result to the original problem is anticipated based on the discussions made above. The flow chart of iteration procedure is illustrated in Fig. 4.

5. Implementation through Abaqus user subroutine UEL

5.1. Finite element discretization in UEL

In order to take the advantage of the powerful pre-process system and the nonlinear solver in Abaqus [55], the above phase field model is implemented by using the Abaqus user subroutine UEL. Here a quadrilateral element with 4 nodes is defined. And at each node there are 3 degrees of freedom (i.e. u_x, u_y and d). For the iteration approach proposed in the previous section, the element's tangent stiffness matrix AMATRX and the residual force vector RHS (i.e. right hand side vector) should be specified in the form of

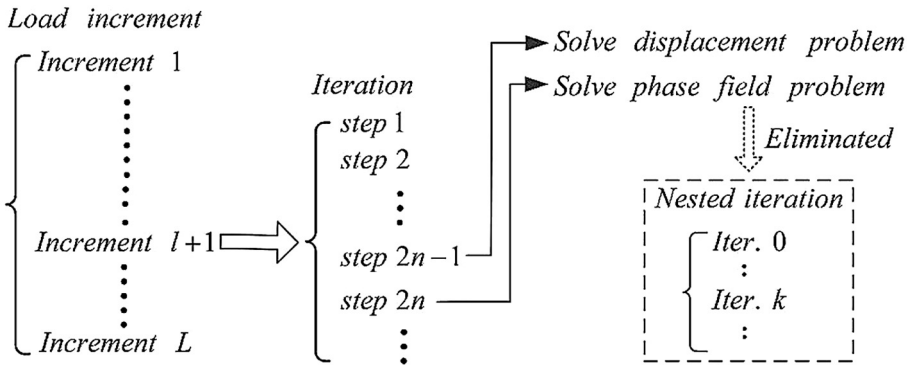

Fig. 4. Flow chart of the improved staggered iteration procedure.

$$\mathbf{AMATRX} = \mathbf{Q}\begin{bmatrix}\mathbf{K}^u & \\ & \mathbf{K}^d\end{bmatrix}\mathbf{Q}^{\mathrm{T}}, \qquad \mathbf{RHS} = \mathbf{Q}\begin{bmatrix}\mathbf{S}^u \\ \mathbf{S}^d\end{bmatrix} \tag{42}$$

where Q is a transform matrix to rearrange the position of these degrees of freedom (DOFs).

In order to guarantee the phase field's irreversibility, a history-depended variable $\mathcal{H}$ defined by Eq. (25) is introduced. This variable can be recorded and accessed by the array SVARS which records the solution-dependent state variables associated with the defined element. The values contained in the array should be updated to be the values at the end of the increment. The implementation detail is referred to the following pseudo code:

```
if  SVARS(i) > max(ψ_i^+,  ψ^0)  then
    H = SVARS(i)
else
    H = max(ψ_i^+,  ψ^0)
    SVARS(i) = H
end if
```

In the proposed iteration scheme of the $(l+1)$th load increment, it is seen that the nested iteration should be stopped for even steps (shown in Fig. 2) and hence the solution procedure should be treated separately in odd and even steps. And in what follows, the superscript $l+1$ will be dropped for the sake of simplicity. For odd steps $2n-1, \quad n = 1, 2, 3...$, the phase field and the displacement should be solved from the following equations

$$\mathbf{u}_{2n} = \mathbf{u}_{2n-1} + [\mathbf{K}^u_{2n-1}(\mathbf{d}_{2n-1})]^{-1}\mathbf{R}^u_{2n-1}(\mathbf{d}_{2n-1}) \tag{43}$$

$$\mathbf{d}_{2n} = \mathbf{d}_{2n-1} + [\mathbf{K}^d_{2n-1}(\mathbf{u}_{2n-1}, d_{2n-1})]^{-1}\widetilde{\mathbf{R}}^d_{2n-1}(\mathbf{u}_{2n-1}, \mathbf{d}_{2n-1}) \tag{44}$$

In this step, the displacement $\mathbf{u}$ should be solved with prescribed phase field d, and the increment of phase field d should be zero since it is fixed. And this requires the residual vector $\widetilde{\mathbf{R}}^d_{2n-1}$ which is the difference between the external force and the RHS vector $\mathbf{S}^d_{2n-1}$ must be equal to zero. This can be done by setting the RHS vector $\mathbf{S}^d_{2n-1}$ to be zero, because the external force of phase field is always zero. In this case, the stiffness matrices $\mathbf{K}^u_{2n-1}$, $\mathbf{K}^d_{2n-1}$ and the RHS vector $\mathbf{S}^u_{2n-1} = -\mathbf{K}^u_{2n-1}\mathbf{u}_{2n-1}$ are given directly, and the RHS vector $\mathbf{S}^d_{2n-1} = 0$ is used.

For even steps, $2n$ $(n = 1, 2, 3...)$, the displacement u is kept unchanged and the phase field d is calculated by

$$\mathbf{u}_{2n+1} = \mathbf{u}_{2n} + [\mathbf{K}^u_{2n}(\mathbf{d}_{2n})]^{-1}\mathbf{R}^u_{2n}(\mathbf{d}_{2n}) \tag{45}$$

$$\mathbf{d}_{2n+1} = \mathbf{d}_{2n} + [\mathbf{K}^d_{2n}(\mathbf{u}_{2n}, \mathbf{d}_{2n})]^{-1}\mathbf{R}^d_{2n}(\mathbf{u}_{2n}, \mathbf{d}_{2n}) \tag{46}$$

From Fig. 2 it can be seen that $(\mathbf{u}_{2n}, \quad \mathbf{d}_{2n})$ is already on curve (a) which means in the present step Eq. (29) is satisfied automatically i.e. $\mathbf{R}^u_{2n}(\mathbf{d}_{2n}) = \mathbf{0}$. Hence the next iteration point must locate on the same vertical line as this one. In this step, the stiffness matrix and RHS vectors are just calculated directly, no special treatment should be done.

In the implementation, it is necessary to record the current iteration step number and this can be done through the Abaqus user subroutine UEXTERNALDB. The variable n representing the iteration number is set to 1 at the beginning of each load increment (i.e. when LOP = 1). And the RHS vector $\mathbf{S}^d_{2n-1}$ is multiplied by a parameter $(1+(-1)^n)/2$ such that the value is set to zero for odd iteration steps and unchanged for even steps.

5.2. Convergence criterion

There are two active fields in the present problem i.e., displacement and phase field. As stated above, they are solved alternatively with the proposed iteration method. A convergent solution of both the fields should be determined for the original problem. At any

iteration step, both of the fields are checked with the same criterion. For a specific field α ($\alpha = \mathbf{u}$ or d), two aspects of the solution are checked. On one hand, the nodal variable (nodal displacement or nodal phase field) is checked according to

$$c^{\alpha}_{\max} \leqslant C^{\alpha}\Delta u^{\alpha}_{\max} \tag{47}$$

where $c^{\alpha}_{\max}$ is the largest correction of the nodal variable in the last iteration while $\Delta u^{\alpha}_{\max}$ is the total increment of the nodal variable during the present load increment. Default value of the tolerance parameter $C^{\alpha} = 10^{-2}$ is adopted. On the other hand, the nodal residual force is checked through the following criterion

$$r^{\alpha}_{\max} \leqslant P^{\alpha}\widetilde{q}^{\alpha} \tag{48}$$

where $r^{\alpha}_{\max}$ is the largest nodal residual force at the present iteration step. $P^{\alpha}\widetilde{q}^{\alpha}$ is a tolerance value evaluated from the time-average value of nodal flux (the terminology "nodal flux" is used in Abaqus user's manual [55], here it represents nodal force or equivalent nodal force of phase field). The parameter $P^{\alpha} = 5 \times 10^{-3}$ is chosen by default. The field α ($\alpha = \mathbf{u}$ or d) is considered convergent only if both of the criterions are satisfied. The final convergence is accepted when convergent solutions for both of the fields are found, otherwise a new iteration step will be performed until the final balance of the system is found.

6. Numerical examples

In this section four examples are given to verify the validity and efficiency of the present implementation and the proposed iteration scheme. In the first three examples both of the crack path and load-displacement curves are compared with other numerical and experimental results. Moreover, the validity of the proposed scheme is demonstrated by the comparisons with the staggered scheme [19] through numerical results, iteration steps, and elapsed total time in the simulations. In the following examples, the external load is applied by displacement controlled form and the load step is divided into 50 sub-steps with the convergent criterion given in Section 5.2. And the simulations are executed on a workstation with Inter (R) Xeon(R) CPU E5-2620 v4 @ 2.10 GHz processor and 128 GB RAM.

6.1. Mode-I failure of three point bending (TPB)

A TPB beam with a notch at the middle of the bottom is considered, and the problem was also studied in Ref. [56]. The beam's geometric configuration and boundary conditions are shown in Fig. 5. The material properties are: Young's modulus $E = 2.0 \times 10^4$ MPa, Poisson's ratio $\upsilon = 0.2$, fracture energy $G_s = 0.113$ N/mm, and failure strength of the cohesive model $f_t = 2.4$ MPa. The parameters characterizing the cohesive relationship is available in Ref. [41] (i.e. $a_2 = 1.3868$ and $a_3 = 0.6567$). The internal length $l_0 = 2.5\,mm$ and a finite element size $h = 0.5\,mm$ around the potential crack path are used in numerical simulation. The load is applied within 50 steps and at each step Δu_y is fixed to 0.02 mm.

This TPB problem is a pure mode-I failure, so it can be certain that the crack will emerge from the top of the notch and then propagate along the symmetric line. The present predicted crack path is shown in Fig. 6(b). Without any *ad-hoc* criterions the crack path is just as expected. And the phase field distribution has a good agreement with Ref. [41] as shown in Fig. 6(a). Theoretically, the value of phase field varies from 0 to 1 represents intact and failure material states, respectively. The value in between 0 and 1 represents material damage. However, from the phase field evolution equation it can be seen that $d = 1$ results in an infinite strain energy density at the point which is physically unreasonable. So a sufficiently big value $d_{\max}$ can be used in practice for example $d_{\max} = 0.8$ was used in Ref. [48]. In the present study, the critical vale is set to be $d_{\max} = 0.95$ which is closer to the ideal value. Hence from Fig. 6(b) it can be seen that the regions of which the phase field values are close to $d_{\max}$ are identified as cracks. Force-displacement curves obtained by the present method, Ref. [41] as well as the experimental tests [56] are illustrated in Fig. 7, and good agreement is found.

Here the staggered scheme proposed in Ref. [19] is also used to investigate the performance of the proposed iteration scheme. The force-displacement curves obtained by the staggered scheme [19] and the proposed scheme are given in Fig. 8. It can be seen that the results are perfectly matches to each other. It means that both of the schemes are valid for the present problem. In Fig. 9, the iteration steps at each load increment of the two schemes are shown, it is seen that the proposed scheme needs less iterations steps. Especially in the third increment, 343 iteration steps and 6.13 min are needed by the staggered scheme [19] while only 118 steps and 2.09 min

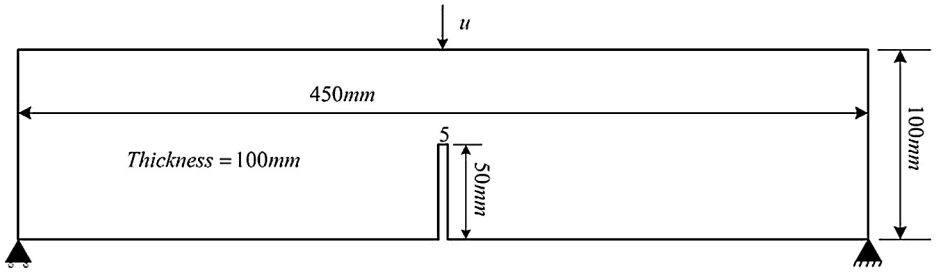

Fig. 5. Geometry of TPB specimen.

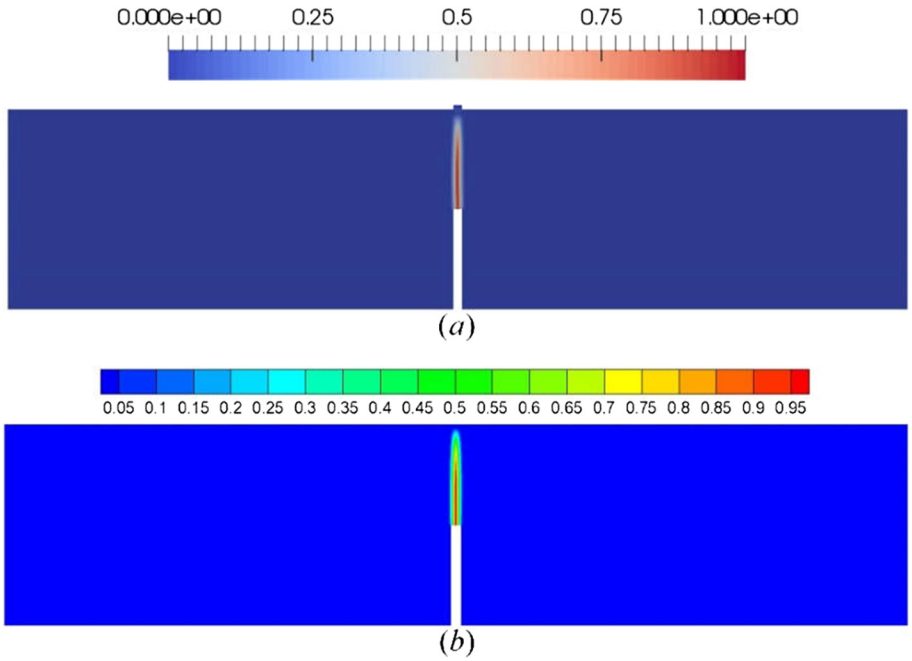

Fig. 6. Crack paths predicted by Ref. [41] (a, Reprinted with permission from Elsevier) and (b) the present simulation.

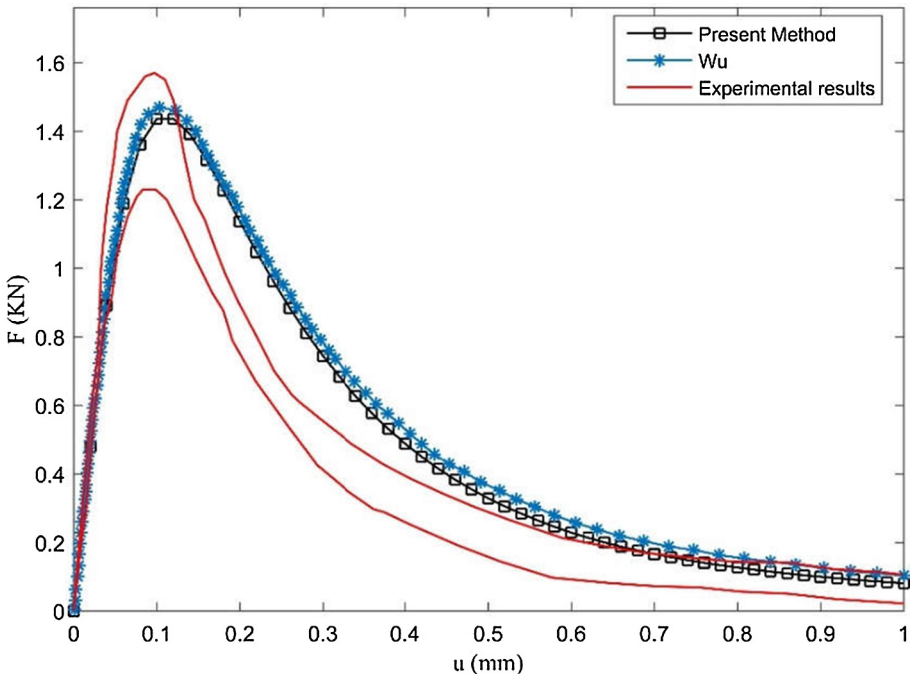

Fig. 7. Force-displacement curves of TPB specimen.

are needed by the present iteration scheme. The time cost by the reference scheme [19] is 184% higher compared to the present one. The total number of the iteration steps and the elapsed time of the two schemes are listed in Table 1. The existing staggered scheme [19] requires nearly 2 times of the computational time of the proposed one.

6.2. *Mixed-mode failure of TPB*

A mixed-mode failure of three point bending test is considered and the corresponding experimental evidence is reported in Ref.

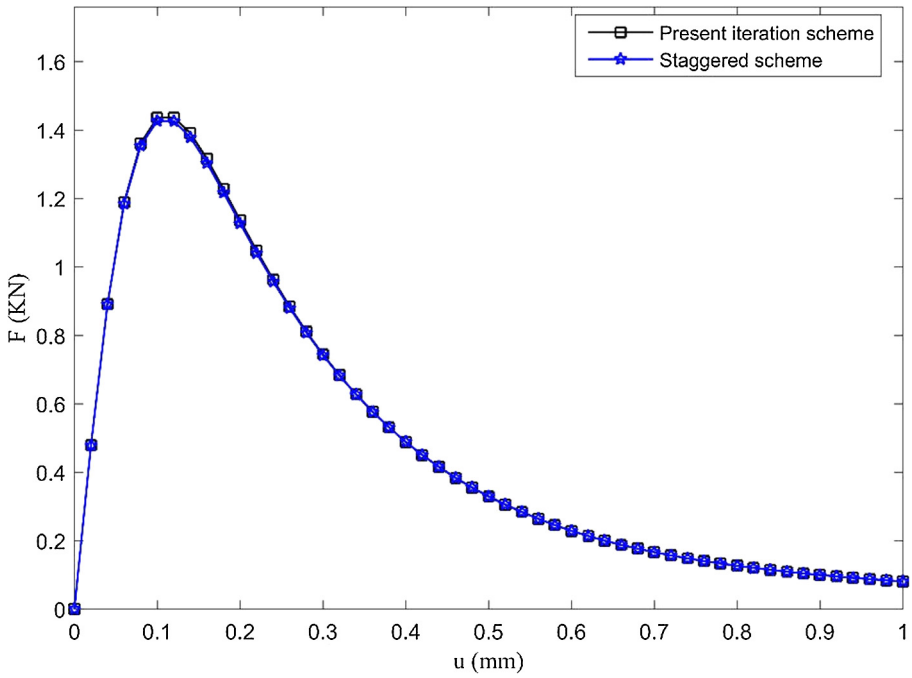

Fig. 8. Force-displacement curves obtained by different schemes.

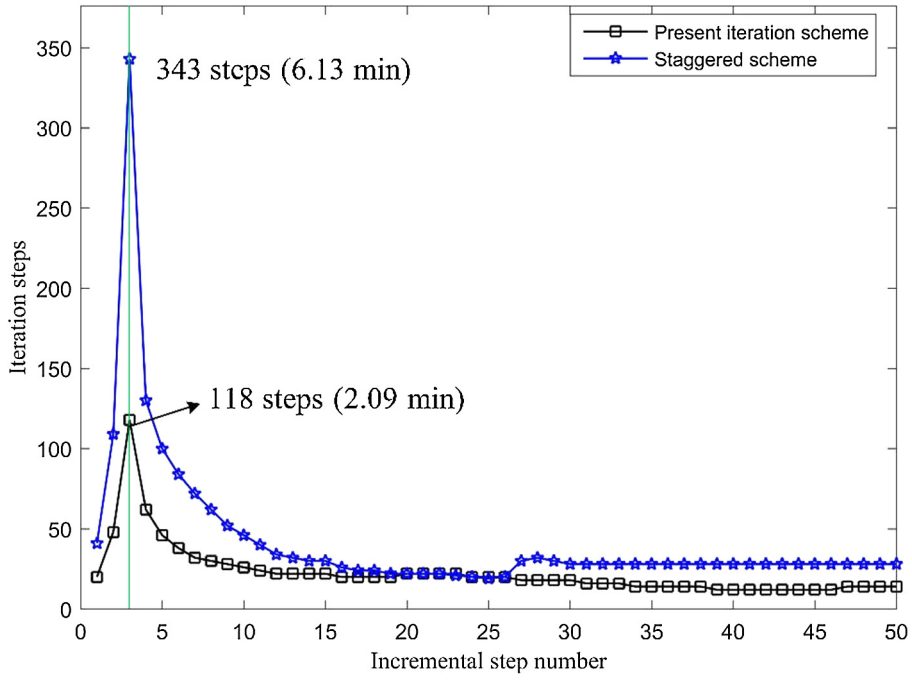

Fig. 9. Comparison of iteration steps at each load increment.

Table 1
Comparisons of the total number of iteration steps and elapsed time.

Schemes	Total number of iteration steps	Elapsed time
Present iteration scheme	1130	20 min
Staggered scheme [19]	2127	38 min

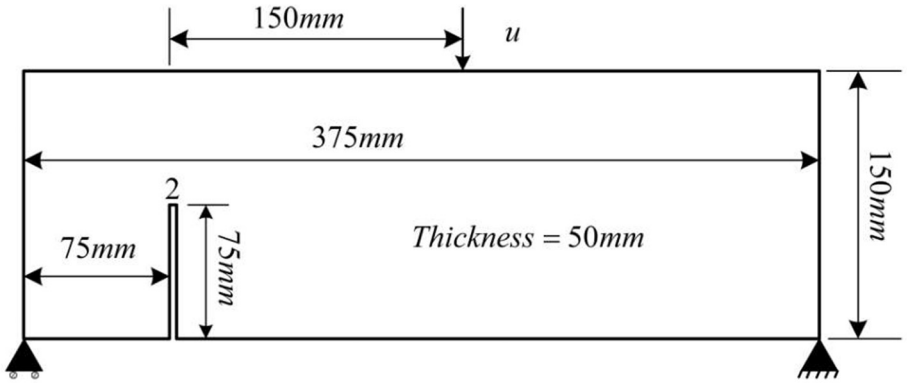

Fig. 10. Geometry of mixed-mode failure TPB.

[57]. As shown in Fig. 10, the size of the specimen is 375 mm × 150 mm × 50 mm, with a 2mm wide notch at the bottom of the beam. The material properties are specified by: Young's modulus $E = 3.8 \times 10^4$ MPa, Poisson's ratio $\upsilon = 0.2$, fracture energy $G_s = 0.069$ N/mm and tensile strength $f_t = 3.0$ MPa. The model parameters are chosen as $a_2 = 1.3868$ and $a_3 = 0.6567$. And the length scale $l_0 = 1.5$ mm and finite element size $h = 0.3$ mm along the potential crack path are used during the numerical simulation. The displacement loading is applied within 50 incremental steps and at each step Δu_y is fixed to 0.003 mm.

This problem is subjected to a mixed-mode failure. The range of experimental crack paths [57] is depicted in Fig. 11(a). Fig. 11(b) and (c) are the crack paths predicted by Ref. [42] and the present method. Just as in the previous example, the regions in which phase field value is close to 0.95 are identified as crack. It can be seen from figure that the predicted crack path matches very well with the experimental data. The predicted force versus crack mouth opening displacement (CMOD) curves are illustrated in Fig. 12. The results obtained by the present method is in good agreement with Ref. [42]. And both of them are in accordance with the

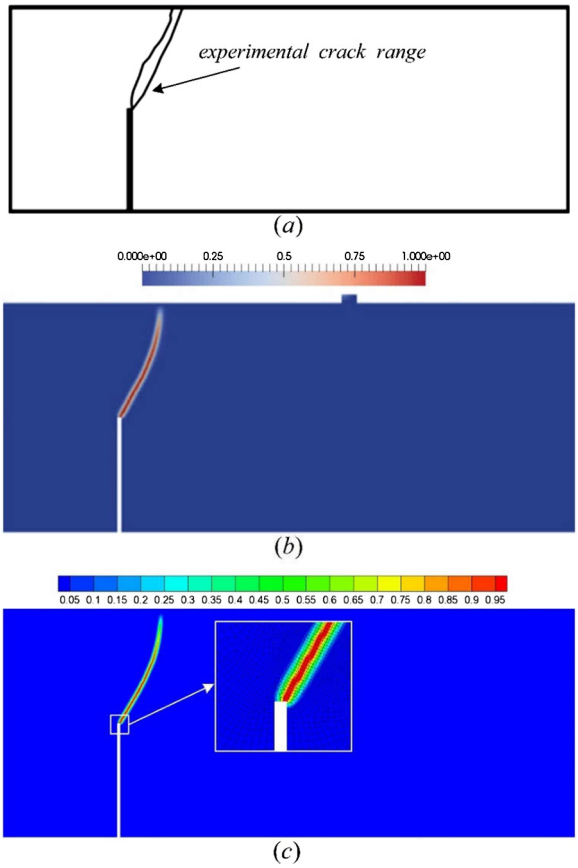

Fig. 11. Crack paths given by (a) experiment [57], (b, Reprinted with permission from Elsevier) Wu [42] and (c) the present simulation.

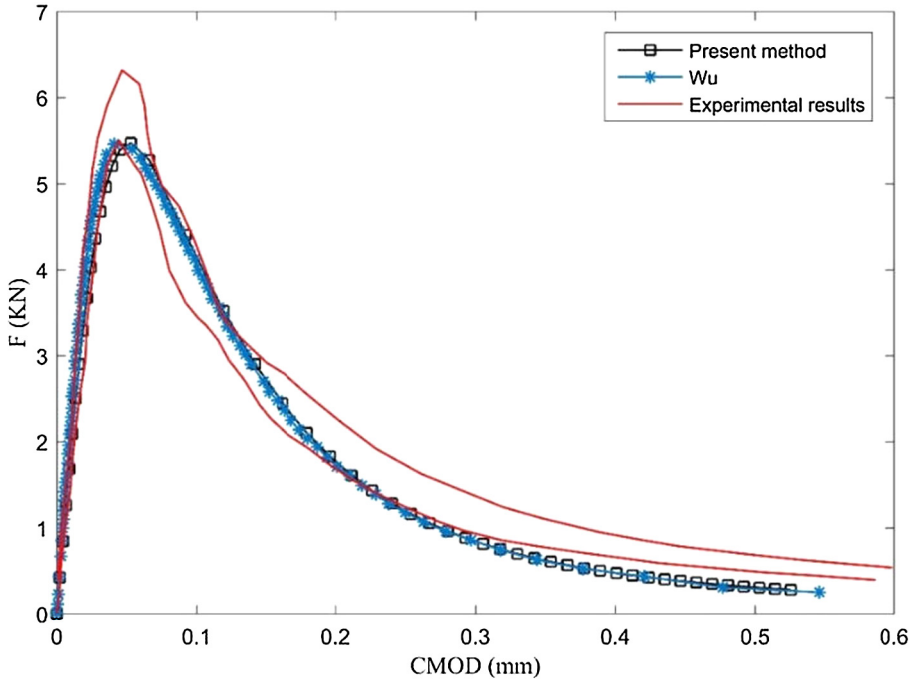

Fig. 12. Force-CMOD curves of the specimen.

experimental results [57].

In Fig. 13, the Force-CMOD curves obtained by the proposed scheme and staggered scheme [19] are given. The results are identical with each other. In Fig. 14 which illustrates the iteration steps at each loading increment by using different schemes, it is clear that less iteration steps are needed in the proposed iteration scheme. Especially in the 17th incremental loading step the total iteration steps and elapsed time are 240 and 2.26 min for the staggered scheme while by using the proposed scheme only 142 steps and 1.32 min are required. The same phenomenon also can be observed from the rest incremental steps. The total number of the

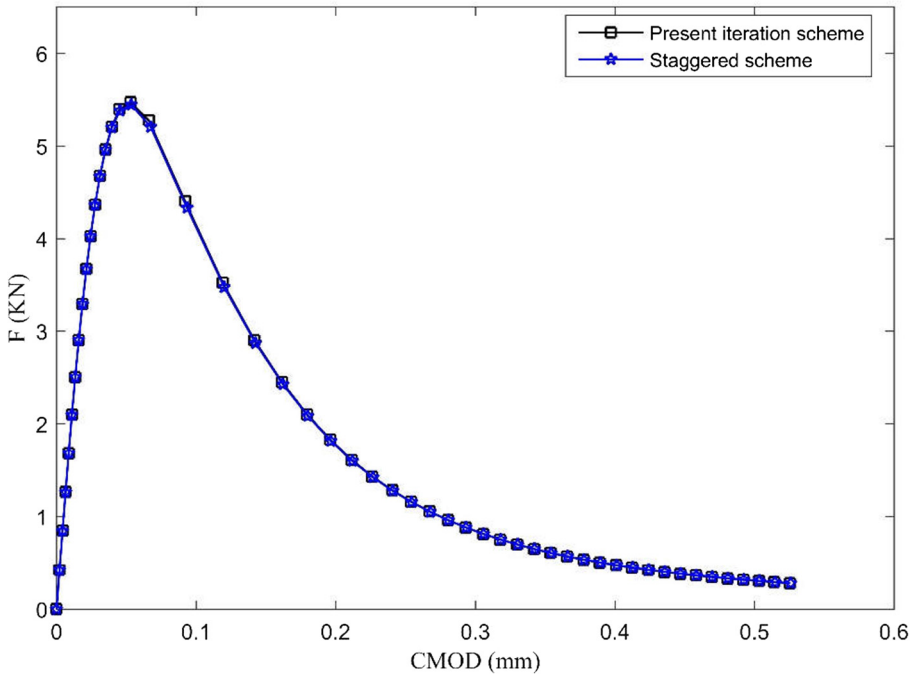

Fig. 13. Force-CMOD curves obtained by different schemes.

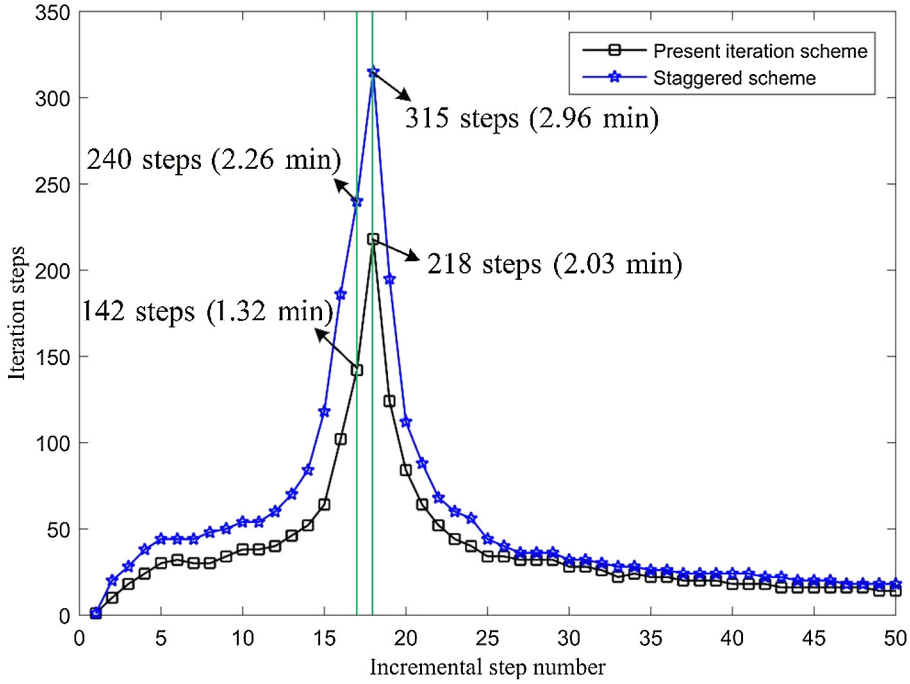

Fig. 14. Comparison of iteration steps at each load increment.

Table 2
Comparisons of the total number of iteration steps and elapsed time.

Schemes	Total number of iteration steps	Elapsed time
Present iteration scheme	1931	18 min
Staggered scheme [19]	2767	26 min

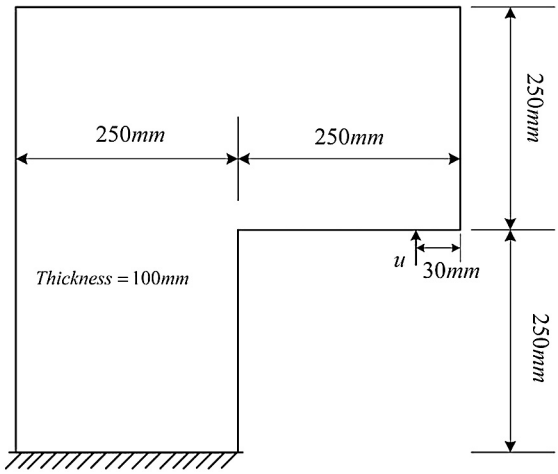

Fig. 15. Geometry of L-shaped panel.

iteration steps and the elapsed time of the two schemes are listed in Table 2. It can be observed that the staggered scheme [19] needs about 1.5 times of the elapsed time of the proposed scheme.

6.3. Mixed-mode failure of L-shaped panel

In the present example, a mixed-mode failure of L-shape panel conducted by Ref. [58] is considered. The geometry and boundary

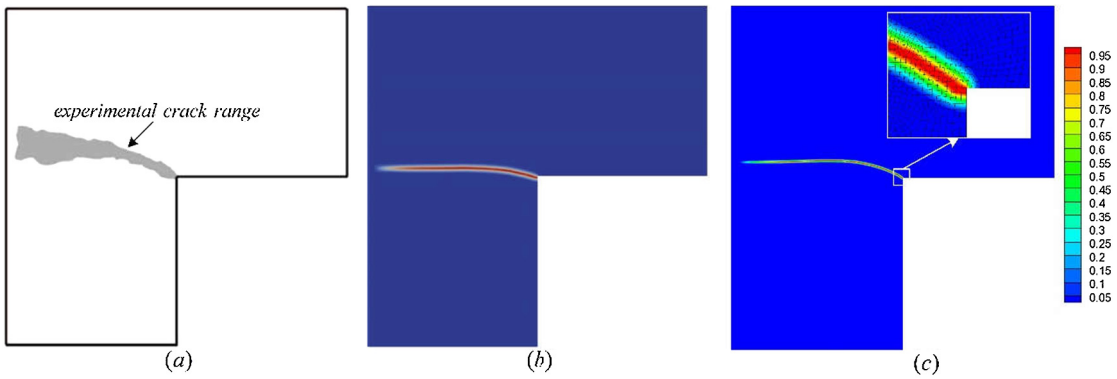

Fig. 16. Crack paths given by (a) experiment [58], (b, Reprinted with permission from Elsevier) Wu [42] and (c) the present simulation.

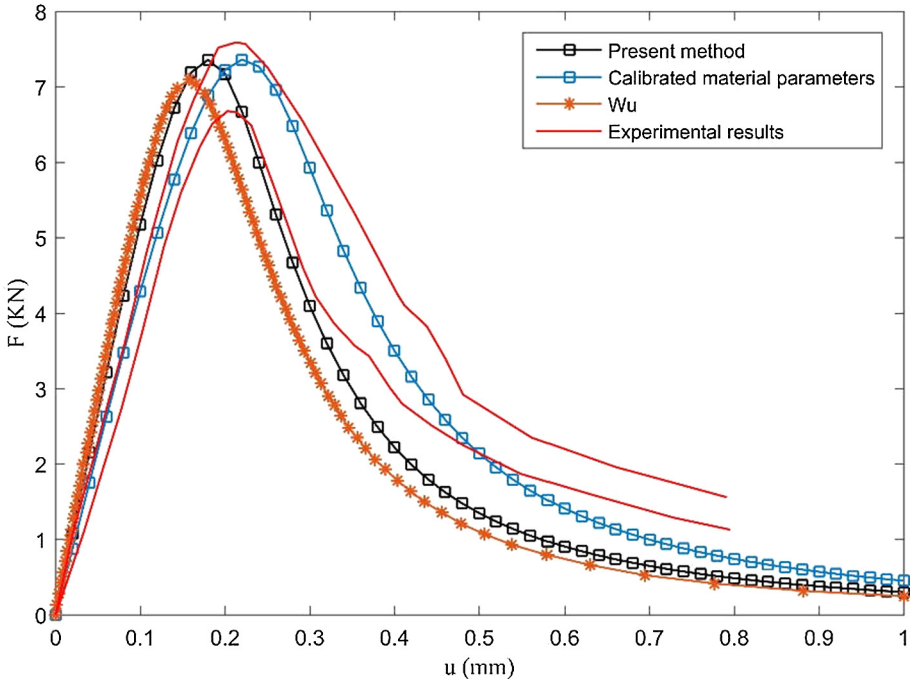

Fig. 17. Force-displacement curves of the specimen.

conditions are shown in Fig. 15. The bottom of the specimen is applied with a prescribed displacement at the point at 30mm to the right side. The load is applied by 50 incremental steps and at each step Δu_y is fixed to 0.02 mm. And the following material properties and model parameters are used: Young's modulus $E = 2.528 \times 10^4$ MPa, Poisson's ratio $\upsilon = 0.18$, fracture energy $G_s = 0.09$ N/mm, failure strength $f_t = 2.7$ MPa, $a_2 = 1.3868$ and $a_3 = 0.6567$. And in the numerical simulation the internal length scale $l_0 = 2$ mm and finite element size of $h = 0.5$ mm along the potential crack path are used.

Fig. 16(a) illustrates the range of the experimental crack paths [58]. The crack paths predicted by Ref. [42] and the present method are shown in Fig. 16(b) and (c). Good agreement can be found through the comparing of the figures. The force-displacement curves obtained in Ref. [42] and the present study are illustrated in Fig. 17. Both of them are matching with the experiment results [58]. It should be noted that the initial stiffness of the structure is overestimated by using the above material properties. So in order to obtain a solution which is more closely to the experimental results, modified material parameters are suggested in Refs. [10,59,60]. And in the present example the calibrated material parameters i.e. $E = 21$ GPa and $G_s = 0.13$ N/mm, suggested by Nguyen et al. [10] are adopted. The corresponding force-displacement curve is depicted in Fig. 17. It can be observed that the curve is more tallied with the experimental data. In Fig. 18, the force-displacement curves obtain by the staggered scheme [19] and the proposed iteration scheme are given. Similar with the previous examples both of the schemes are valid for the problem. In Fig. 19 the iteration steps at each incremental load are shown. It can be seen that the required iteration steps of all the incremental loading by using the proposed scheme are less than the staggered scheme [19]. Especially in the 10th and 12th incremental loading steps as shown in the figure, the staggered scheme [19] requires about twice iteration steps and elapsed time than the proposed scheme. The total number of the

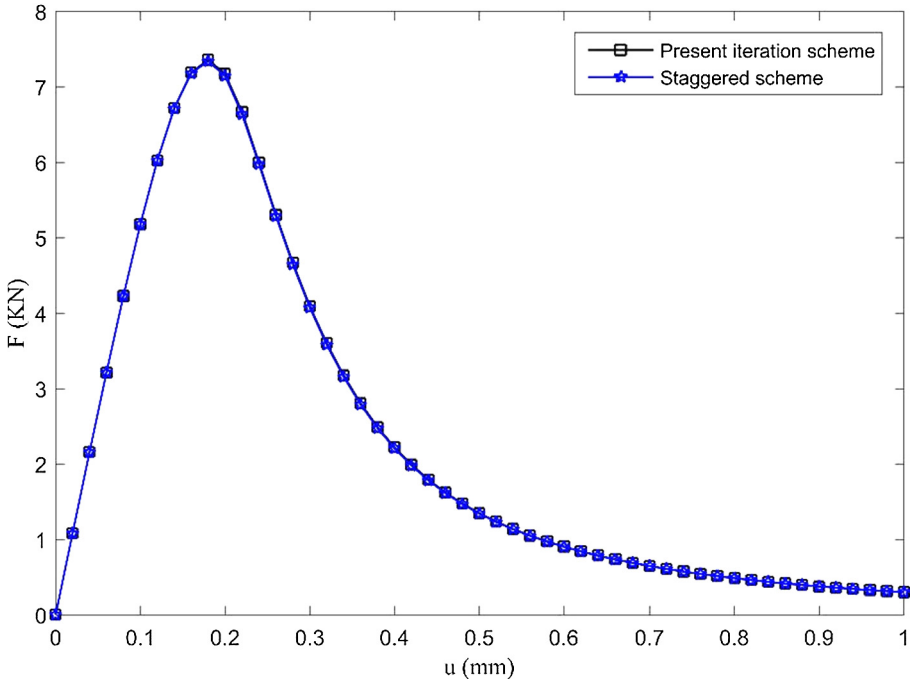

Fig. 18. Force-displacement curves obtained by different schemes.

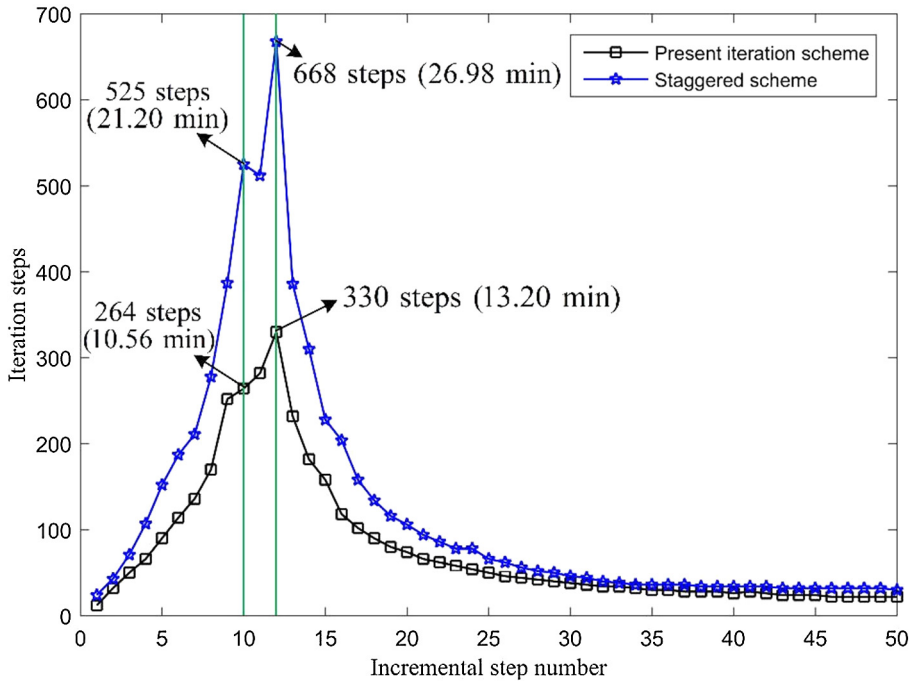

Fig. 19. Comparison of iteration steps at each load increment.

Table 3
Comparisons of the total number of iteration steps and elapsed total time.

Schemes	Total number of iteration steps	Elapsed total time
Present iteration scheme	3876	155 min
Staggered scheme [19]	6165	249 min

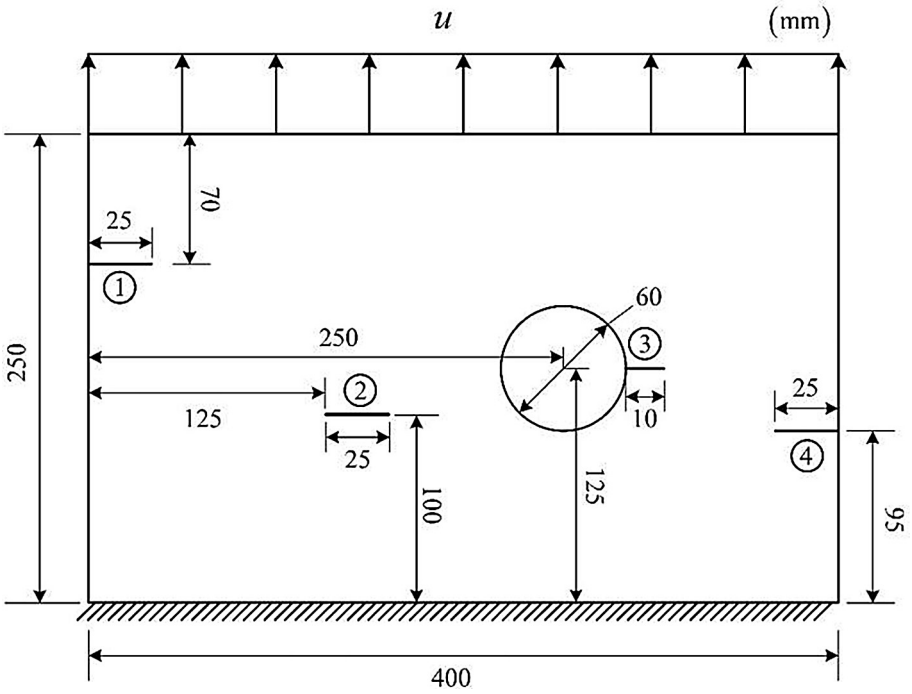

Fig. 20. Geometry and boundary conditions of the plate with a hole and multiple cracks.

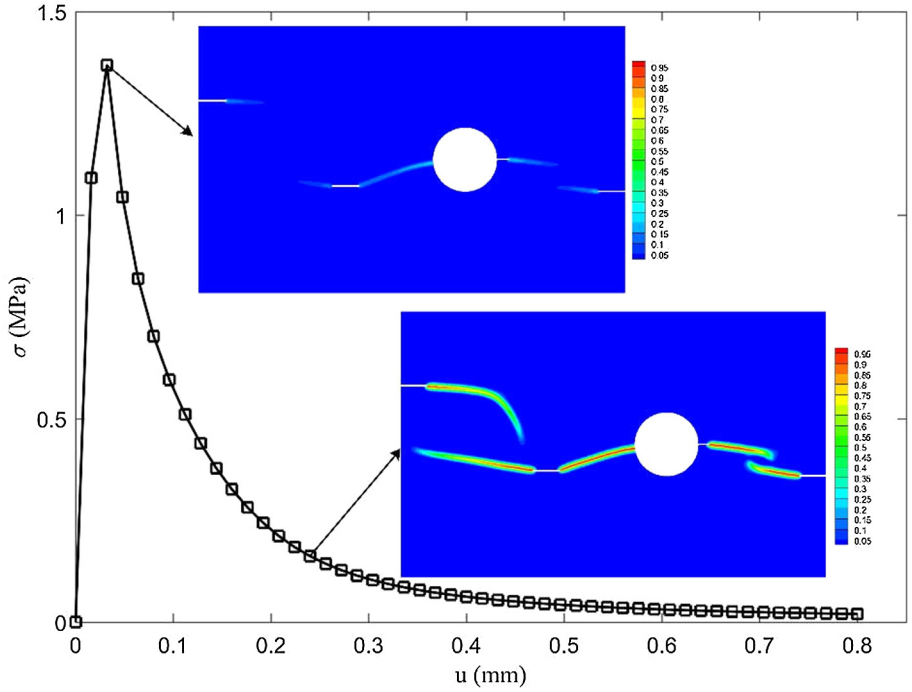

Fig. 21. Mechanical response curve and crack patterns under at $u = 3.2 \times 10^{-2}$ mm and $u = 0.24$ mm.

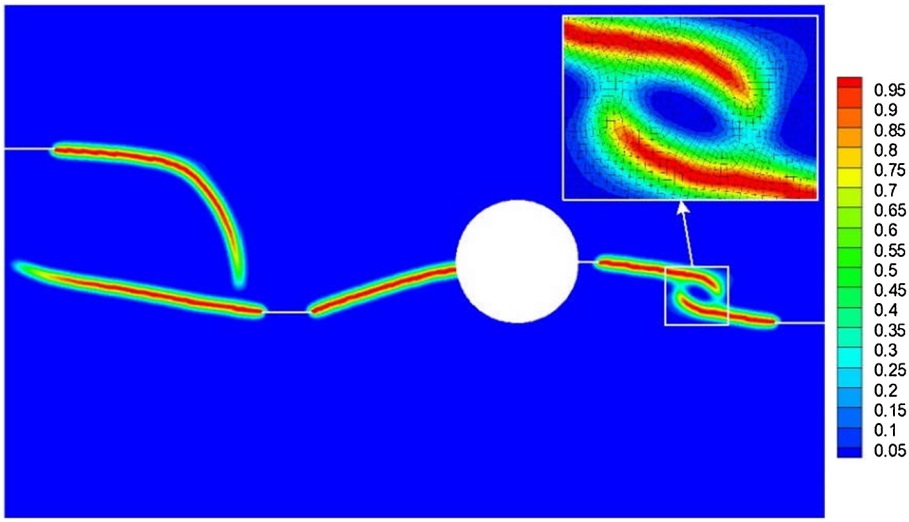

Fig. 22. Ultimate crack pattern of the plate.

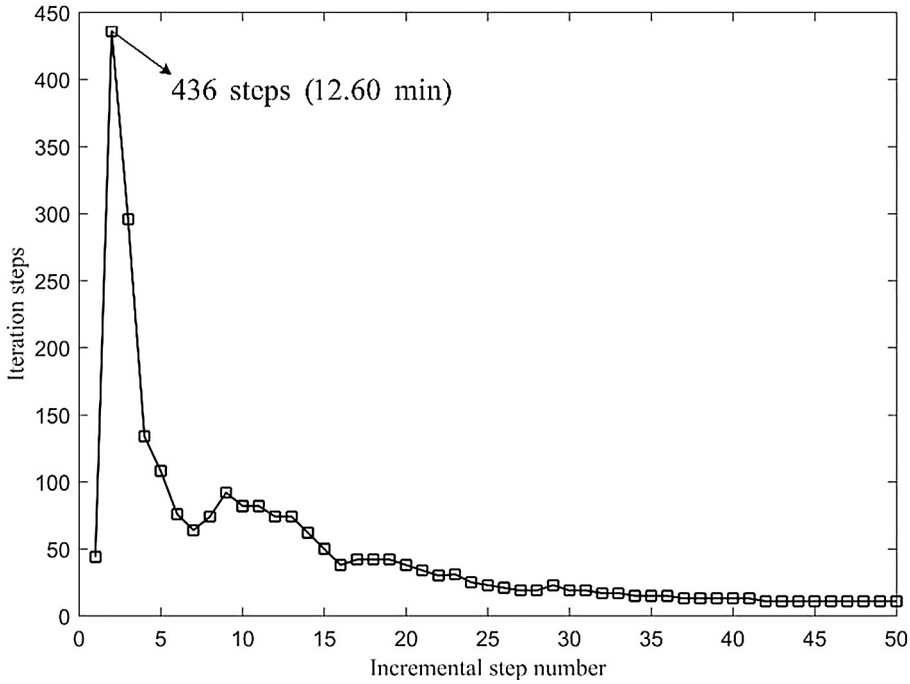

Fig. 23. Iteration steps at each incremental loading.

iteration steps and the elapsed time of the two schemes are listed in Table 3. It can be seen that the staggered scheme [19] needs about 1.5 times more computational costs compared with the proposed scheme.

6.4. Plate with a hole and multi-cracks

In this example the validity of the present implementation and algorithm is illustrated through complex fracture in a plate with four initial cracks and a hole. The geometry and boundary conditions of the plate are shown in Fig. 20. The material properties and model parameters are as follows: Young's modulus $E = 20\,\text{GPa}$, Poisson's ratio $\upsilon = 0.2$, fracture energy $G_s = 0.13\,\text{N/mm}$, failure strength $f_t = 2.5\,\text{MPa}$, $a_2 = 1.3868$ and $a_3 = 0.6567$. Fine elements with effective size $h = 1.0\,\text{mm}$ are set along the potential crack paths and the corresponding internal length scale are specified as $l_0 = 3.5\,\text{mm}$. The present simulation is performed with displacement controlled incremental loadings of $\Delta u = 1.6 \times 10^{-2}\,\text{mm}$.

In this simulation both of the existing staggered scheme [19] and the proposed scheme are considered. The total iteration steps

and elapsed computational time of the proposed scheme are 2456 steps and 71 min. However, by using the staggered scheme [19] at the second incremental loading a convergent solution cannot be obtained even after 2500 iteration attempts, which means a convergence issue exists in this circumstance. Since the problem is considered under the same environment i.e. load increment, error tolerance and other parameters, it indicates that the proposed iteration scheme has higher robustness than the existing staggered scheme. According to the results shown below, five cracks are nucleated at this instant and this sudden change might be the main reason of the convergence issue of the existing staggered scheme. The mechanical response curve and crack patterns at two specified stages i.e. $u = 3.2 \times 10^{-2}$ mm and $u = 0.24$ mm are depicted in Fig. 21. The stress σ is calculated by dividing all the nodal forces of the nodes on the upper boundary by the specimen width. It can be observed that the reaction stress reaches the maximum value at $u = 3.2 \times 10^{-2}$ mm. Five cracks are nucleated at this instant. Then with the increasing of the loading the cracks start to propagation and the external stress decreases. Fig. 22 shows the ultimate crack pattern at $u = 0.8$ mm. It is interesting to find that the two cracks on the right side of the hole are trending to merge to each other. The curve of the number of iteration steps at each incremental loading is depicted in Fig. 23. It is observe that at the unstable instant $u = 3.2 \times 10^{-2}$ mm the present scheme also requires the most iteration steps (436 steps and 12.60 min).

7. Conclusions

In the present paper, a unified phase field model for cohesive fracture with hybrid (isotropic-anisotropic) formula is used to simulate quasi-brittle problems. The model is implemented by using Abaqus user subroutine UEL (user defined element). Many aspects of the model and the implementation techniques are discussed in details. Moreover, an iteration scheme for phase field models for cohesive fracture with high efficiency is proposed. This iteration scheme degenerates to the widely used staggered scheme when brittle fracture is considered. The validity of the present implementation and the iteration scheme is demonstrated by numerical examples. Comparisons on total iteration steps and the elapsed total computational time are also made between the proposed iteration scheme and the existing scheme, and results have shown that the proposed iteration scheme is vary suitable for the phase field model when cohesive fracture problem is considered.

8. Appendix

Supplementary material associated with this study can be downloaded from:
http://pan.dlut.edu.cn/share?id=jq1s6tsdr94s or
https://drive.google.com/open?id=1LYZFeBWje5ht26IUj7hhepgVcrUbIIn8.

Acknowledgements

This work was supported by the National Natural Science Foundation of China (Nos. 11372065, 11502045), and the National Key Research and Development Program of China [No. 2016YFB0200702].

References

[1] Borst RD. Numerical aspects of cohesive-zone models. Engng Fract Mech 2003;70:1743–57.
[2] Zhou F, Molinari JF. Dynamic crack propagation with cohesive elements: a methodology to address mesh dependency. Int J Numer Meth Engng 2004;59:2000–6.
[3] Sukumar N, Moës N, Moran B, Belytschko T. Extended finite element method for three-dimensional crack modelling. Int J Numer Meth Engng 2015;48:1549–70.
[4] Moës N, Belytschko T. Extended finite element method for cohesive crack growth. Engng Fract Mech 2002;69:813–33.
[5] de Borst R, Verhoosel CV. Gradient damage vs phase-field approaches for fracture: similarities and differences. Comput Meth Appl Mech Engng 2016;312:78–94.
[6] Peerlings Rd, De Borst R, Brekelmans Wd, De Vree J. Gradient enhanced damage for quasi-brittle materials. Int J Numer Meth Engng 1996;39:3391–403.
[7] Comi C. Computational modelling of gradient-enhanced damage in quasi-brittle materials. Mech Cohesive-Friction Mater: Int J Exper Modell Comput Mater Struct 1999;4:17–36.
[8] Peerlings R, Geers M, De Borst R, Brekelmans W. A critical comparison of nonlocal and gradient-enhanced softening continua. Int J Solids Struct 2001;38:7723–46.
[9] Pham K, Amor H, Marigo J-J, Maurini C. Gradient damage models and their use to approximate brittle fracture. Int J Damage Mech 2011;20:618–52.
[10] Nguyen TH, Bui TQ, Hirose S. Smoothing gradient damage model with evolving anisotropic nonlocal interactions tailored to low-order finite elements. Comput Meth Appl Mech Engng 2018;328:498–541.
[11] Francfort GA, Marigo JJ. Revisiting brittle fracture as an energy minimization problem. J Mech Phys Solids 1998;46:1319–42.
[12] Griffith AA. The phenomena of rupture and flow in solids. Philos Trans R Soc Lond 1921;221:163–98.
[13] Bourdin B, Francfort GA, Marigo JJ. The variational approach to fracture. Springer Science+Business Media B.V; 2008.
[14] Kuhn C, Müller R. A continuum phase field model for fracture. Engng Fract Mech 2010;77:3625–34.
[15] Miehe C, Hofacker M, Welschinger F. A phase field model for rate-independent crack propagation: robust algorithmic implementation based on operator splits. Comput Meth Appl Mech Engng 2010;199:2765–78.
[16] Ambati M, Gerasimov T, Lorenzis LD. A review on phase-field models of brittle fracture and a new fast hybrid formulation. Comput Mech 2015;55:383–405.
[17] Msekh MA, Sargado JM, Jamshidian M, Areias PM, Rabczuk T. Abaqus implementation of phase-field model for brittle fracture. Comput Mater Sci 2015;96:472–84.
[18] Zhang X, Sloan SW, Vignes C, Sheng D. A modification of the phase-field model for mixed mode crack propagation in rock-like materials. Comput Meth Appl Mech Engng 2017;322:123–36.
[19] Molnár G, Gravouil A. 2D and 3D Abaqus implementation of a robust staggered phase-field solution for modeling brittle fracture. Finite Elem Anal Des 2017;130:27–38.
[20] Alessi R, Marigo J-J, Vidoli S. Gradient damage models coupled with plasticity: variational formulation and main properties. Mech Mater 2015;80:351–67.
[21] Ambati M, De Lorenzis L. Phase-field modeling of brittle and ductile fracture in shells with isogeometric NURBS-based solid-shell elements. Comput Meth Appl Mech Engng 2016;312:351–73.

[22] Ambati M, Gerasimov T, De Lorenzis L. Phase-field modeling of ductile fracture. Comput Mech 2015;55:1017–40.
[23] Borden MJ, Hughes TJ, Landis CM, Anvari A, Lee IJ. A phase-field formulation for fracture in ductile materials: Finite deformation balance law derivation, plastic degradation, and stress triaxiality effects. Comput Meth Appl Mech Engng 2016;312:130–66.
[24] Duda FP, Ciarbonetti A, Sánchez PJ, Huespe AE. A phase-field/gradient damage model for brittle fracture in elastic–plastic solids. Int J Plast 2015;65:269–96.
[25] Miehe C, Hofacker M, Schänzel L-M, Aldakheel F. Phase field modeling of fracture in multi-physics problems. Part II. Coupled brittle-to-ductile failure criteria and crack propagation in thermo-elastic–plastic solids. Comput Meth Appl Mech Engng 2015;294:486–522.
[26] Larsen CJ, Ortner C, Süli E. Existence of solutions to a regularized model of dynamic fracture. Math Models Meth Appl Sci 2010;20:1021–48.
[27] Bourdin B, Larsen CJ, Richardson CL. A time-discrete model for dynamic fracture based on crack regularization. Int J Fract 2011;168:133–43.
[28] Borden MJ, Verhoosel CV, Scott MA, Hughes TJ, Landis CM. A phase-field description of dynamic brittle fracture. Comput Meth Appl Mech Engng 2012;217:77–95.
[29] Hofacker M, Miehe C. Continuum phase field modeling of dynamic fracture: variational principles and staggered FE implementation. Int J Fract 2012;178:113–29.
[30] Schlüter A, Willenbücher A, Kuhn C, Müller R. Phase field approximation of dynamic brittle fracture. Comput Mech 2014;54:1141–61.
[31] Steinke C, Özenç K, Chinaryan G, Kaliske M. A comparative study of the r-adaptive material force approach and the phase-field method in dynamic fracture. Int J Fract 2016;201:97–118.
[32] Liu G, Li Q, Msekh MA, Zuo Z. Abaqus implementation of monolithic and staggered schemes for quasi-static and dynamic fracture phase-field model. Comput Mater Sci 2016;121:35–47.
[33] Bleyer J, Roux-Langlois C, Molinari J-F. Dynamic crack propagation with a variational phase-field model: limiting speed, crack branching and velocity-toughening mechanisms. Int J Fract 2017;204:79–100.
[34] Doan DH, Bui TQ, Duc ND, Fushinobu K. Hybrid phase field simulation of dynamic crack propagation in functionally graded glass-filled epoxy. Compos B Engng 2016;99:266–76.
[35] Doan DH, Bui TQ, Van Do T, Duc ND. A rate-dependent hybrid phase field model for dynamic crack propagation. J Appl Phys 2017;122:115102.
[36] Wu J-Y, Nguyen VP, Nguyen CT, Sutula D, Bordas S, Sinaie S. Phase field modeling of fracture. Adv Appl Mech: Multi-scale Theory Comput 2018;52.
[37] Verhoosel CV, De Borst R. A phase-field model for cohesive fracture. Int J Numer Meth Engng 2013;96:43–62.
[38] Linse T, Hennig P, Kästner M, Borst R. A convergence study of phase-field models for brittle fracture. Engng Fract Mech 2017;184:307–18.
[39] Conti S, Focardi M, Iurlano F. Phase field approximation of cohesive fracture models. Annales De Linstitut Henri Poincaré 2015;33:1033–67.
[40] Freddi F, Iurlano F. Numerical insight of a variational smeared approach to cohesive fracture. J Mech Phys Solids 2017;98:156–71.
[41] Wu JY. A unified phase-field theory for the mechanics of damage and quasi-brittle failure. J Mech Phys Solids 2017;103:72–99.
[42] Wu JY. A geometrically regularized gradient-damage model with energetic equivalence. Comput Meth Appl Mech Engng 2017;328:612–37.
[43] Wu J-Y. Robust numerical implementation of non-standard phase-field damage models for failure in solids. Comput Meth Appl Mech Engng 2018;340:767–97.
[44] Bourdin B, Chambolle A. Implementation of an adaptive finite-element approximation of the Mumford-Shah functional. Numer Math 2000;85:609–46.
[45] Miehe C, Welschinger F, Hofacker M. Thermodynamically consistent phase-field models of fracture: variational principles and multi-field FE implementations. Int J Numer Meth Engng 2010;83:1273–311.
[46] Feng D-C, Wu J-Y. Phase-field regularized cohesive zone model (CZM) and size effect of concrete. Engng Fract Mech 2018;197:66–79.
[47] Wu J-Y, Nguyen VP. A length scale insensitive phase-field damage model for brittle fracture. J Mech Phys Solids 2018;119:20–42.
[48] Nguyen VP, Wu J-Y. Modeling dynamic fracture of solids with a phase-field regularized cohesive zone model. Comput Meth Appl Mech Engng 2018;340:1000–22.
[49] Lancioni G, Royer-Carfagni G. The variational approach to fracture mechanics. A practical application to the French Panthéon in Paris. J Elast 2009;95:1–30.
[50] Amor H, Marigo JJ, Maurini C. Regularized formulation of the variational brittle fracture with unilateral contact: numerical experiments. J Mech Phys Solids 2009;57:1209–29.
[51] Wu J-Y, Cervera M. A novel positive/negative projection in energy norm for the damage modeling of quasi-brittle solids. Int J Solids Struct 2018;139:250–69.
[52] Bourdin B, Marigo J-J, Maurini C, Sicsic P. Morphogenesis and propagation of complex cracks induced by thermal shocks. Phys Rev Lett 2014;112:014301.
[53] Tanne E, Li T, Bourdin B, Marigo JJ, Maurini C. Crack nucleation in variational phase-field models of brittle fracture. J Mech Phys Solids 2018;110:80–99.
[54] Cornelissen HAW, Hordijk DA, Reinhardt HW. Experimental determination of crack softening characteristics of normalweight and lightweight concrete. Delft University of Technology; 1986.
[55] Simulia DCS. Abaqus 6.11 analysis user's manual; 2011.
[56] Rots JG. Computational modeling of concrete fracture. Phdthesis Delft University of Technology; 1988.
[57] Gálvez JC, Elices M, Guinea GV, Planas J. Mixed mode fracture of concrete under proportional and nonproportional loading. Int J Fract 1998;94:267–84.
[58] Winkler BJ. Traglastuntersuchungen von unbewehrten und bewehrten Betonstrukturen auf der Grundlage eines objektiven Werkstoffgesetzes für Beton. Phdthesis Delft University of Technology; 2001.
[59] Unger JF, Eckardt S, Könke C. Modelling of cohesive crack growth in concrete structures with the extended finite element method. Comput Meth Appl Mech Engng 2007;196:4087–100.
[60] Zamani A, Gracie R, Reza Eslami M. Cohesive and non-cohesive fracture by higher-order enrichment of XFEM. Int J Numer Meth Engng 2012;90:452–83.